Nanoscale Friction of High Entropy Alloy Sulfide Thin Films in Comparison with Molybdenum Disulfide

Gokay Adabasi¹, Aditya Deshpande², Koichi Tanaka², Joshua Ancheta¹, Emmanuel Maldonado¹, Mehmet Özdoğan¹, Suneel Kodambaka^{2,3,a)} and Mehmet Z. Baykara^{1,a)}

¹Department of Mechanical Engineering, University of California Merced, Merced, California 95343, USA

²Department of Materials Science and Engineering, University of California Los Angeles, Los Angeles, California 90095, USA

³Department of Materials Science and Engineering, Virginia Polytechnic Institute and State University, Blacksburg, Virginia 24061, USA

We present nanoscale friction measurements performed on sputter-deposited high entropy alloy (HEA) sulfide thin films ((VNbTaMoW)S₂) via atomic force microscopy. Results reveal (i) the influence of deposition time on film morphology and (ii) the presence of isolated areas of low friction on film surfaces. We compare the friction results on HEA sulfide thin films with those on a prototypical solid lubricant, sputter-deposited molybdenum disulfide (MoS₂), and find that they are superior in terms of lubricative performance. Variable temperature X-ray diffraction, performed up to 973 K, reveals that HEA sulfide thin films exhibit improved oxidation resistance when compared with MoS₂ films. Combined, our results show that HEA sulfide thin films have considerable potential as oxidation-resistant solid lubricant coatings.

a) Authors to whom correspondence should be addressed: kodambaka@vt.edu, mehmet.baykara@ucmerced.edu

High entropy alloys (HEAs),¹ consisting of five or more principal elements in similar ratios, are gaining rapid attention from the scientific community thanks to their intriguing combination of mechanical properties with high thermal and chemical stability.² While the exact physical mechanisms that lead to this attractive suite of material properties are still under active investigation, it is established that the "high entropy effect" prevents the formation of intermetallic compounds and thus leads to simple solid solutions, and that significant lattice distortion plays a role in improving mechanical strength and limiting mass transport in the form of diffusion.³

While a significant portion of HEA research is devoted to the bulk form of these materials, HEAs exhibit significant potential to be employed as mechanical component coatings in thin film form, specifically for applications where mechanical strength and wear resistance are required in combination with thermal and chemical resistance. Consequently, several recent studies have been performed to evaluate the structural, mechanical and tribological properties of HEA thin films.⁴ In particular, HEA thin films have been generally found to exhibit high wear resistance⁵ as well as high temperature stability⁶ and in certain cases, relatively low friction.⁷ On the other hand, the question of whether HEA thin films can act as effective solid lubricant coatings (i.e. exhibit low friction) under dry contact conditions has not been investigated yet from a fundamental point of view. Specifically, a nanoscale analysis of the structure-friction relationship in HEA thin films, which could enable the rational design of solid lubricant HEA coatings, is lacking.

Motivated as above, we present here nanoscale imaging and friction measurements performed on thin films of (VNbTaMoW)S₂, an HEA sulfide, by way of atomic force microscopy (AFM). The concept of entropic stabilization has been applied to compounds (borides,⁸ carbides,⁹ nitrides,^{10,11} and oxides¹²) with five or more cations. Recent density functional theory (DFT) calculations¹³ of transition-metal alloy disulfides, with five cations selected from nine of the group

4-6 transition-metals, predict that the alloy disulfides are energetically stable. Other studies have suggested that HEA transition-metal dichalcogenides are likely to exhibit superior properties and attractiveness for a variety of applications. 14-22

Our results reveal that HEA sulfide thin films exhibit a non-uniform morphology whereby isolated areas of low friction are surrounded by areas of relatively high friction. Remarkably, the overall friction values measured on HEA thin films are lower than those measured on MoS₂ thin films, supporting their potential to be used as solid lubricant coatings in mechanical applications. Complementary measurements of X-ray diffraction (XRD) at variable temperatures additionally show that HEA sulfide thin films exhibit superior oxidation resistance than MoS₂, with implications of applicability in harsh environmental conditions.

The (VNbTaMoW)S₂ and MoS₂ thin films are grown via magnetron sputter-deposition of a 50.8 mm diameter circular equiatomic HEA (VNbTaMoW) target (Plasmaterials Inc.) and a Mo (99.95%, Plasmaterials Inc.) target, respectively, using an ultra-high vacuum (UHV) deposition chamber. $^{23-25}$ A 2×10×0.5 mm³ Al₂O₃(0001) substrate is cleaned by ultrasonication for 10 minutes sequentially in acetone, isopropanol, and deionized water, and blow-dried with nitrogen gas. The substrate is then mounted to a heating stage. The substrate/stage assembly is introduced into a load-lock chamber, which is pumped down to ~ 10^{-8} Torr, and then transferred to a UHV chamber. The substrate is degassed at 1273 K until the base pressure $p_{\rm B}$ is below 6×10⁻⁹ Torr. The substrate temperature $T_{\rm S}$ is set to 1073 K. The HEA sulfide films and MoS₂ films are deposited for different deposition times (between t = 9 minutes and 60 minutes) in 1% H₂S/Ar gas mixture, with a total gas pressure of 20 mTorr.

The AFM measurements were performed under ambient conditions using a commercial AFM instrument (Asylum Research, Cypher VRS) and cantilever (Nanosensors, PPP-CONTR).

The normal and lateral calibration of the cantilever was performed by the Sader²⁶ and the wedge methods,²⁷ respectively. During all measurements, the scanning frequency was 1 Hz, and the applied normal load was zero, which resulted in a purely adhesive contact between the tip and the sample. Measurements were performed in contact mode, and maps of topography were recorded simultaneously with maps of lateral force, from which friction maps were generated.²⁸ Characterization experiments complementary to AFM included scanning electron microscopy (SEM) imaging (Zeiss, GeminiSEM 500), as well as XRD performed at variable temperatures (Bede, D1 diffractometer equipped with a non-monochromatic Cu X-ray source).

In order to investigate the overall morphology of the HEA sulfide thin films, SEM imaging was performed. As shown in the representative image of Fig. 1(a), films exhibit a grainy morphology, with nearly homogenously dispersed grains of lateral size on the order of a few tens of nanometers. The occasional presence of elevated, flat regions that are a few hundreds of nanometers in lateral span is also noted (see the white arrow in Fig. 1(a)); the three-dimensional morphology of these is analyzed via AFM in the following parts of the manuscript. While the respective morphologies are quite different, the co-existence of two structurally distinct features on the films are reminiscent of a similar observation that was previously made on sputter-deposited films of (VNbTaMoW)N, an HEA nitride. Additionally, recent growth experiments have revealed that sputter-deposited (VNbTaMoW)S $_x$ thin films are layered and composed of a homogenous mixture of transition metal disulfides VS $_2$, NbS $_2$, TaS $_2$, MoS $_2$ and WS $_2$.

To draw conclusions about the crystalline structure of the (VNbTaMoW)S₂ thin films, XRD was performed. Fig. 1(b) is a representative XRD spectrum obtained from an HEA sulfide thin film deposited for t = 30 minutes. In the spectrum, strong peaks are observed at 14.6°, 29.2°, 44.3°, and 60.0°, which we attribute to 0002l (with l = 1, 2, 3, ...) reflections of hexagonal-

structured transition metal disulfide phases indicating that the sulfide phase is 0001-oriented. In addition to the basal plane reflections, a weak peak from $10\overline{1}0$ is observed at 31.6°. The 0001-oriented growth is commonly observed in other transition metal disulfide materials such as $MoS_2^{23,30}$ and HEA sulfides.²⁹

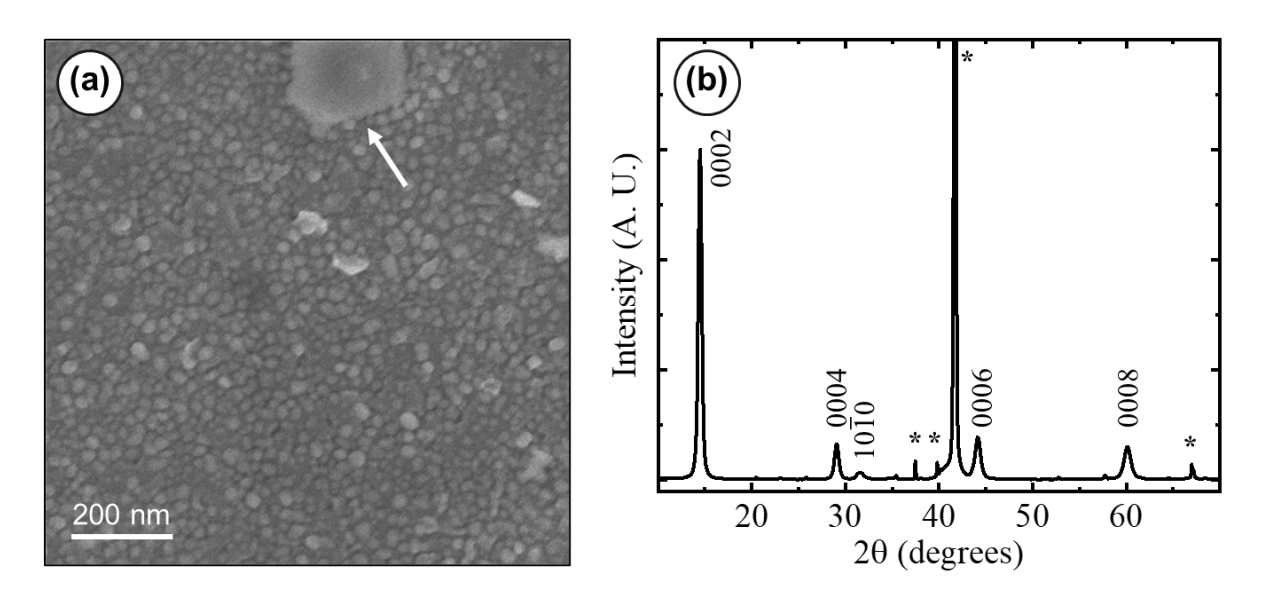


FIG 1. (a) Representative SEM image of the (VNbTaMoW)S₂ thin film sputter-deposited on Al₂O₃(0001). The overall morphology is grainy, with the isolated presence of elevated flat regions (white arrow). (b) Typical XRD scan acquired from the (VNbTaMoW)S₂ thin film. Peaks from HEA sulfide phases are indexed as shown. Asterisks denote reflections from the Al₂O₃(0001) substrate.

Following the global structural characterization of (VNbTaMoW)S₂ thin films via SEM and XRD as described in Fig. 1, we performed AFM experiments to investigate their topographical and frictional characteristics on a local level. AFM experiments were performed on two types of (VNbTaMoW)S₂ thin films, grown over a time span of 60 min and 9 min. Fig. 2 shows a summary of AFM results obtained on the 60-min (VNbTaMoW)S₂ thin films. In particular, Fig. 2(a,b) confirms the morphological conclusions drawn from the SEM image in Fig. 1(a), in the sense that

the overall morphology seems to consist of a nearly homogenously dispersed grainy background, broken by the presence of isolated flat regions, i.e., plateaus, with a lateral span of a few hundreds of nanometers. Line profiles drawn over the plateaus (Fig. 1(c)) show that they are several tens of nanometers in height (up to ~60 nm), whereas the overall RMS roughness of the topography map in Fig. 2(b) is calculated as 13.2 nm. The friction map shown in Fig. 1(d), which is recorded simultaneously with the topography map in Fig. 1(b), comprises an interesting observation. The plateau regions exhibit significantly lower friction than the surrounding grainy background (with mean values of 0.44 nN and 1.85 nN, respectively).

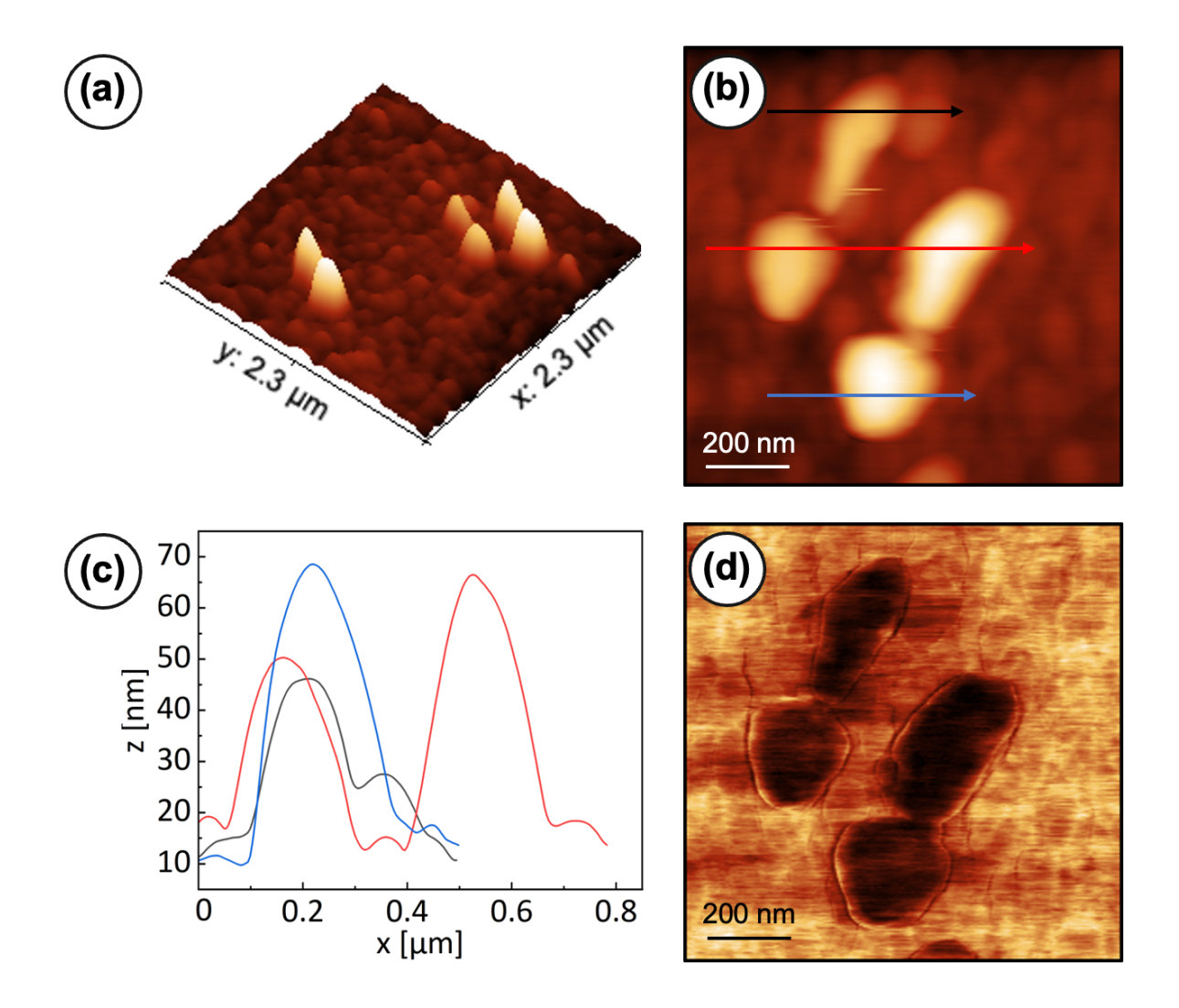


FIG 2. (a) Three-dimensional (3D) representation of a topographical AFM map acquired on the 60-min (VNbTaMoW)S₂ thin film. Contrast range: 0-64.4 nm. (b) Zoomed-in topographical map on two of the plateaus observed in (a). Contrast range: 0-72.3 nm. (c) Line profiles along the three directions shown with black, red, and blue lines in (b). (d) Friction map acquired simultaneously with the topographical map in (b). Contrast range: 0.16-3.01 nN.

To evaluate the effect of deposition time on the topographical and frictional characteristics of the films, AFM measurements were repeated on the 9-min (VNbTaMoW)S₂ samples (Fig. 3). In particular, it is observed that the 9-min films exhibit a significantly smoother morphology when compared with 60-min films. Specifically, while the overall morphology is still grainy, and

elevated regions (i.e., plateaus) can still be observed (Fig. 3(a,b)), these are much more shallow when compared with their counterparts in the 60-min films (on the order of a few nanometers high, up to \sim 10 nm; please see line profiles presented in Fig. 1(c)) and laterally span smaller distances (up to \sim 150 nm). The former observation is supported by roughness calculations; the overall RMS roughness value of the topography map in Fig. 3(b) is calculated as 2.0 nm, nearly an order of magnitude smoother than the 60-min (VNbTaMoW)S₂ film. On the other hand, it is again observed here that the elevated regions exhibit lower friction than the surroundings, although the contrast between the two regions is less significant when compared with the 60-min films (with mean values of 1.21 nN and 2.03 nN, respectively).

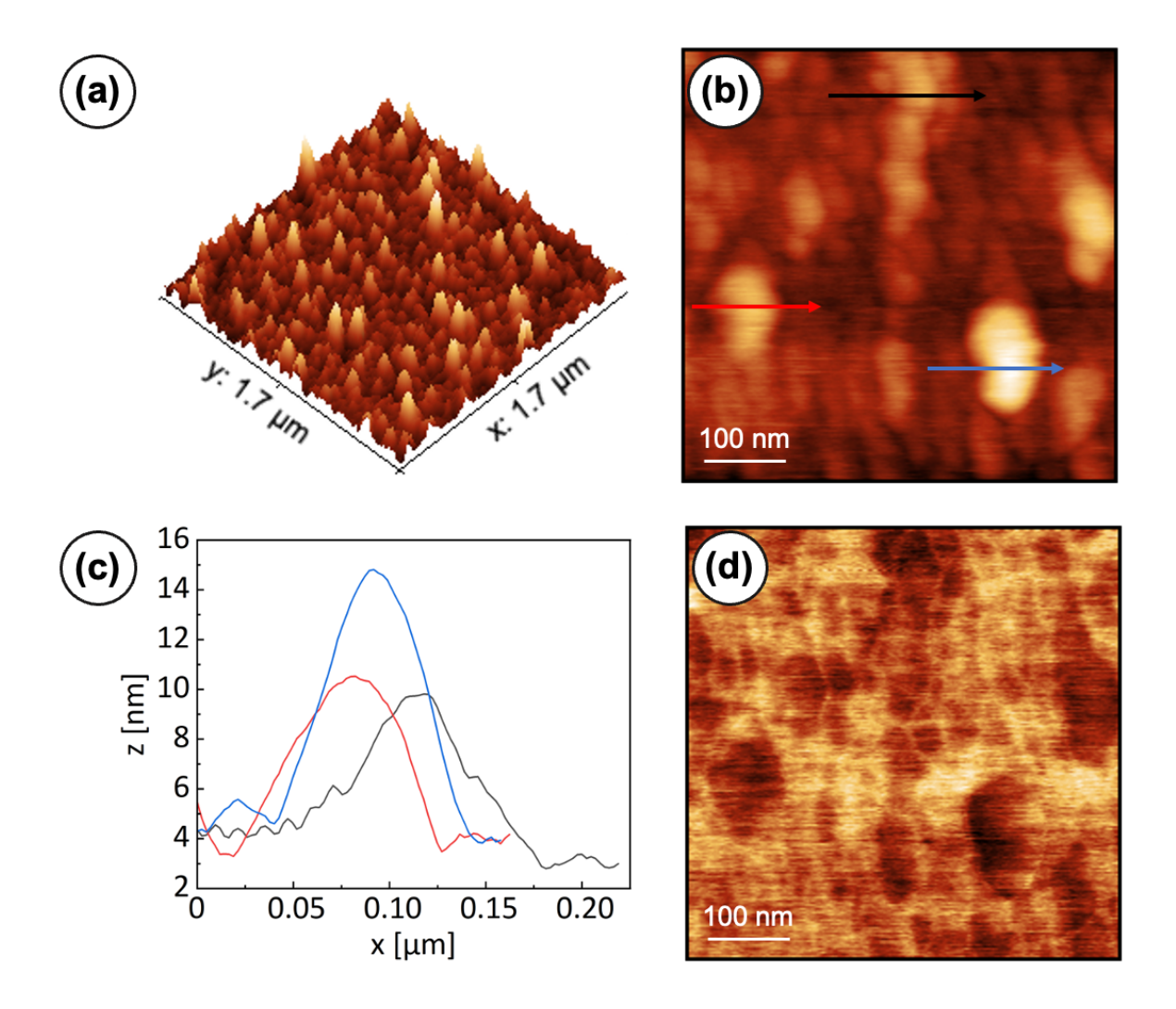


FIG 3. (a) 3D representation of a topographical AFM map acquired on the 9-min (VNbTaMoW)S₂ thin film. Contrast range: 0 - 12.6 nm. (b) Zoomed-in topographical map on the region shown in (a). Contrast range: 0 - 14.5 nm. (c) Line profiles along the three directions shown with black, red, and blue lines in (b). (d) Friction map acquired simultaneously with the topographical map in (b). Contrast range: 0.83 - 2.56 nN.

It has been established that actual friction force values recorded in nanotribology experiments such as the ones presented here bear little value by themselves, specifically because they are a strong function of the structure and chemistry of the tip apex. 31,32 As such, in order to understand whether the friction force values measured on the HEA sulfide thin films are indicative of solid lubricative characteristics, we performed comparative experiments on sputter-deposited MoS₂ thin films, the results of which are presented in Fig. 4. It is particularly interesting to note here that the sputter-deposited MoS₂ films also exhibit a granular morphology, again highlighted by the presence of extended plateaus up to ~100 nm in height (Fig. 4(a,b)) and several hundreds of nanometers in lateral span. Perhaps more interestingly, plateau regions on MoS₂ films also exhibit lower friction when compared with the surrounding areas (with mean values of 10.7 nN and 20.4 nN, respectively), quite reminiscent of the results obtained on 60-min (VNbTaMoW)S₂ thin films. Remarkably, the range of friction forces recorded on the MoS₂ thin film, which is a prototypical solid lubricant system, are higher than both types of HEA sulfide thin films studied here.

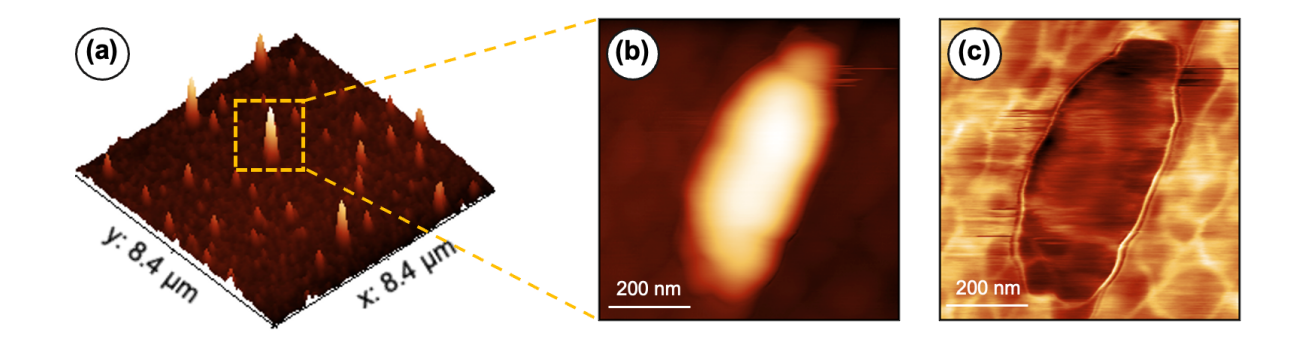


FIG 4. (a) 3D representation of a topographical AFM map acquired on the sputter-deposited MoS_2 thin film. Contrast range: 0-89.8 nm. (b) Zoomed-in topographical map of the highlighted area in (a), focusing on a single plateau. Contrast range: 0-78.5 nm. c) Friction map acquired simultaneously with the topographical map in (b). Contrast range: 3.1-30.2 nN.

Complementing the fundamental topographical and frictional characterization of the HEA sulfide and MoS₂ thin films, we performed variable temperature XRD (VT-XRD) measurements to gauge the high temperature oxidation resistance of the two types of materials in a comparative fashion (Fig. 5). In these measurements, HEA sulfide and MoS₂ thin film samples deposited for t = 30 minutes were used. In both samples, peaks are observed at 14.6° , 29.2° , 44.3° , and 60.0° , which we attribute to 0002l (with l = 1, 2, 3, ...) reflections due to hexagonally-structured transition metal disulfide phases. In addition to the basal plane reflections, the HEA sulfide thin film shows another peak from $10\overline{1}0$ at 31.6° . In both samples, the peak intensities of the sulfide phases remain uniform below 673 K and then decrease at higher temperatures, presumably due to oxidation of the sulfide phase. The onset of the decay is observed at around 773 K for the MoS₂ thin film along with the emergence of a new peak at 25.2° (labeled with \mathbf{o}), which we attribute to either 040 of α -MoO₃ (JCPDS 05-0508) or 210 of h-MoO₃ (JCPDS 21-0569). In contrast, the HEA sulfide thin film exhibits a higher onset temperature for oxidation, at around 873 K. The result suggests

superior oxidation resistance of HEA thin films when compared with MoS₂ and as such, improved potential for tribological applications at elevated temperatures.

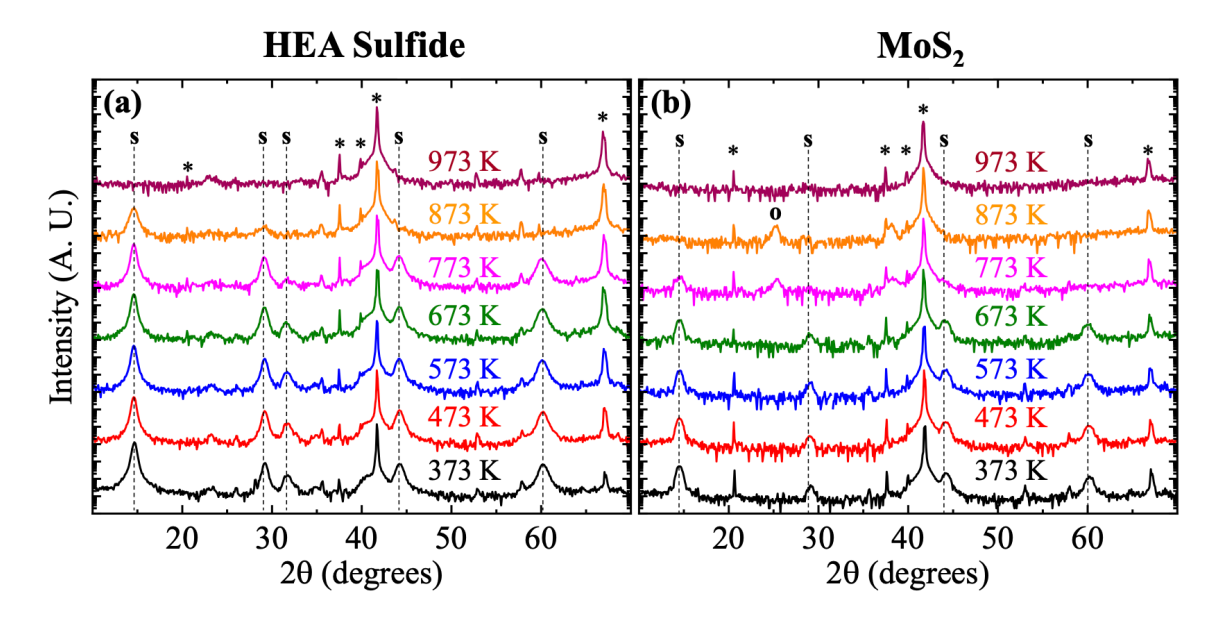


FIG 5. Variable temperature XRD scans obtained from (a) HEA sulfide and (b) MoS_2 thin films sputter-deposited on $Al_2O_3(0001)$ substrates for 30 min. Intensities are plotted on a logarithmic scale. Reflections from hexagonally-structured transition metal disulfide phases and $Al_2O_3(0001)$ substrates are denoted by **s** and asterisk, respectively. In the MoS_2 thin film sample, the peak at 25.2°, presumably from the oxide phase MoO_3 , is labeled as **o**.

At this point, it is important to re-iterate that direct comparisons of friction force values obtained on different samples via AFM need to be exercised with great caution, as minute chemical and structural changes of the tip apex (e.g., those induced by molecular adsorption and tip wear, respectively) can affect the value of the recorded friction forces, even on the same sample, to a significant extent.^{31,32} As such, in order to test whether substantial tip changes occurred during the course of our comparative friction measurements, we performed a control experiment. In particular, friction values were recorded on a mechanically exfoliated MoS₂ flake deposited on a SiO₂ substrate (i) before and (ii) after the set of consecutive measurements on the 60-min and 9-

min (VNbTaMoW) S_2 thin films and the sputter-deposited MoS₂ thin film. The mean friction force values obtained on the exfoliated MoS₂ test flake before and after the measurements were 0.06 nN and 0.05 nN, respectively. This confirms the validity of the comparative nanoscale friction analysis presented here as it shows that no substantial tip change took place during the experiments reported here.

A consistent observation associated with the results presented here (for both types of (VNbTaMoW)S₂ thin films) is the presence of elevated plateau regions with low friction compared to their surroundings. Potential reasons for this observation could include (i) a lower degree of roughness on the plateau regions, (ii) varying chemical composition for the plateau regions when compared with the surrounding, grainy background, and lastly, (iii) a more "ordered" structure owing to different mode of growth for the plateau regions when compared with the grainy background. Measurements of topographical roughness performed on the plateau vs. grainy regions (with representative values of 7.3 nm and 4.7 nm for Fig. 2(b), respectively) do not explain the observed friction trends. On the other hand, it needs to be pointed out that the observation of elevated plateau regions with low friction is not exclusive to the (VNbTaMoW)S₂ thin films and the same observation was also made for the sputter-deposited MoS₂ thin films studied here (see Fig. 4(c)). Consequently, it is unlikely that differences in chemical composition are the main factor that leads to attenuated friction on plateaus of HEA sulfide thin films. Having said this, the literature on sputter-deposited MoS₂ thin films includes frequent discussion of columnar vs. layerby layer growth (or transitions between the two structures) with the latter being attributed to as the low-friction configuration due to ease of sliding between extended layers stacked parallel on top of each other.^{33–35} Consequently, a likely scenario could involve that the HEA sulfide thin films studied here also grow in a similar fashion to MoS₂, whereby isolated regions of layer-by-layer

growth (i.e., the plateaus) are surrounded by regions of columnar growth (i.e., the grainy background) with the former yielding lower friction values in a similar mechanism to MoS₂ thin films. While recent XRD experiments support the idea of a layered morphology for HEA sulfide films,²⁹ more experiments (e.g., cross-sectional SEM imaging) would need to be performed to further validate or refute this potential explanation. On the other hand, the observation of a less significant friction contrast between plateaus and grainy background on the 9-min (VNbTaMoW)S₂ thin film when compared with the 60-min version, when evaluated together with the observation that plateaus are much more shallow on 9-min (VNbTaMoW)S₂ thin film, support the idea of the formation of an ordered, layer-by-layer structure during extended film deposition playing the major role in friction measurements. Specifically, a longer deposition time would lead to the formation of higher, more extended plateau regions and the stacking of more HEA sulfide planes on top of each other, resulting in attenuated friction.

While the results presented here are promising with respect to the potential of (VNbTaMoW)S₂ thin films as high temperature, oxidation-resistant solid lubricant coatings, more work needs to be done to further explore this potential. In particular, a thorough characterization of wear characteristics on small length scales would be needed, in addition to the friction results here, to reach a complete nanotribological understanding. Another point to note is that MoS₂ performs best as a solid lubricant under conditions of low humidity and vacuum.³⁴ As such, repeat measurements performed under dry nitrogen, or even vacuum conditions would be needed to determine if the favorable solid lubrication characteristics of (VNbTaMoW)S₂ over MoS₂ in thin film form would carry over to these operating conditions. Finally, thin films of sulfides of other HEA compositions need to be investigated with AFM, in order to determine if the sulfide formation is the key contributor to the solid lubricative performance observed here.

Acknowledgments

We acknowledge support from the Air Force Office of Scientific Research (AFOSR, Dr. Ali Sayir) via Grant Nos. FA9550-18-1-0050 and FA9550-20-1-0184. Support is also acknowledged by the Merced nAnomaterials Center for Energy and Sensing (MACES) via the National Aeronautics and Space Administration (NASA) Grant Nos. NNX15AQ01 and NNH18ZHA008CMIROG6R. S.K. acknowledges the National Science Foundation (NSF) for DMR Award No. 2211350 (Dr. James Edgar). K.T. was supported by the Japanese Student Service Organization (L16111111026) and the UCLA Department of Materials Science and Engineering (MSE). A.D. was partially supported by UCLA MSE. K.H. was supported by the Japan U.S. Advanced Collaborative Education Program (JUACEP).

References

- ¹ J.W. Yeh, S.K. Chen, S.J. Lin, J.Y. Gan, T.S. Chin, T.T. Shun, C.H. Tsau, and S.Y. Chang, Adv. Eng. Mater. **6**, 299–303 (2004).
- ² E.P. George, D. Raabe, and R.O. Ritchie, Nat. Rev. Mater. **4**, 515–534 (2019).
- ³ D.B. Miracle, and O.N. Senkov, Acta Mater. **122**, 448–511 (2017).
- ⁴ D. Luo, Q. Zhou, Z. Huang, Y. Li, Y. Liu, Q. Li, Y. He, and H. Wang, Coatings 12, 1428 (2022).
- ⁵ C. Sha, Z. Zhou, Z. Xie, and P. Munroe, Appl. Surf. Sci. **507**, 145101 (2020).
- ⁶ S. Zhao, C. Liu, J. Yang, W. Zhang, L. He, R. Zhang, H. Yang, J. Wang, J. Long, and H. Chang, Surf. Coat. Technol. **417**, 127228 (2021).
- ⁷ W.L. Lo, S.Y. Hsu, Y.C. Lin, S.Y. Tsai, Y.T. Lai, and J.G. Duh, Surf. Coat. Technol. **401**, 126247 (2020).
- ⁸ J. Gild, Y. Zhang, T. Harrington, S. Jiang, T. Hu, M.C. Quinn, W.M. Mellor, N. Zhou, K. Vecchio, and J. Luo, Sci. Rep. **6**, 37946 (2016).
- ⁹ T.J. Harrington, J. Gild, P. Sarker, C. Toher, C.M. Rost, O.F. Dippo, C. McElfresh, K. Kaufmann, E. Marin, L. Borowski, P.E. Hopkins, J. Luo, S. Curtarolo, D.W. Brenner, and K.S. Vecchio, Acta Mater. **166**, 271–280 (2019).
- ¹⁰ H. Zaid, K. Tanaka, C. V. Ciobanu, J.M. Yang, S. Kodambaka, and H. Kindlund, Scr. Mater. 197, 113813 (2021).
- ¹¹ H. Zaid, K. Tanaka, M. Liao, M.S. Goorsky, S. Kodambaka, and H. Kindlund, Nano Lett. **21**, 577–582 (2021).
- ¹² C.M. Rost, E. Sachet, T. Borman, A. Moballegh, E.C. Dickey, D. Hou, J.L. Jones, S. Curtarolo, and J.P. Maria, Nat. Commun. **6**, 8485 (2015).
- ¹³ A. Deshpande, C. Ratsch, C. V. Ciobanu, and S. Kodambaka, J. Appl. Phys. **131**, 234302 (2022).
- ¹⁴ J. Cavin, A. Ahmadiparidari, L. Majidi, A.S. Thind, S.N. Misal, A. Prajapati, Z. Hemmat, S. Rastegar, A. Beukelman, M.R. Singh, K.A. Unocic, A. Salehi-Khojin, and R. Mishra, Adv. Mater. **33**, 2100347 (2021).
- ¹⁵ T. Ying, T. Yu, Y.S. Shiah, C. Li, J. Li, Y. Qi, and H. Hosono, J. Am. Chem. Soc. **143**, 7042–7049 (2021).
- ¹⁶ H. Chen, S. Li, S. Huang, L.A. Ma, S. Liu, F. Tang, Y. Fang, and P. Dai, Acta Mater. **222**, 117438 (2022).
- ¹⁷ J. Qu, A. Elgendy, R. Cai, M.A. Buckingham, A.A. Papaderakis, H. de Latour, K. Hazeldine, G.F.S. Whitehead, F. Alam, C.T. Smith, D.J. Binks, A. Walton, J.M. Skelton, R.A.W. Dryfe, S.J. Haigh, and D.J. Lewis, Adv. Sci. **10**, 2204488 (2023).
- ¹⁸ L. Wu and J.P. Hofmann, Curr. Opin. Electrochem. **34**, 101010 (2022).
- ¹⁹ Y. Chen, Z. Tian, X. Wang, N. Ran, C. Wang, A. Cui, H. Lu, M. Zhang, Z. Xue, Y. Mei, P.K. Chu, J. Liu, Z. Hu, and Z. Di, Adv. Mater. **34**, 2270336 (2022).
- ²⁰ S.K. Nemani, M. Torkamanzadeh, B.C. Wyatt, V. Presser, and B. Anasori, Commun. Mater. **4**, 16 (2023).
- ²¹ W. Cheng, J. Liu, J. Hu, W. Peng, G. Niu, J. Li, Y. Cheng, X. Feng, L. Fang, M.S. Wang, S.A.T. Redfern, M. Tang, G. Wang, and H. Gou, Small **19**, 2301915 (2023).

- ²² M.A. Buckingham, B. Ward-O'Brien, W. Xiao, Y. Li, J. Qu, and D.J. Lewis, Chem. Comm. **58**, 8025–8037 (2022).
- ²³ A. Deshpande, K. Hojo, K. Tanaka, P. Arias, H. Zaid, M. Liao, M. Goorsky, and S.K. Kodambaka, ACS Appl. Nano Mater. **6**, 2908-2916 (2023).
- ²⁴ K. Tanaka, A. Aleman, M.E. Liao, Y. Wang, M.S. Goorsky, and S. Kodambaka, Thin Solid Films **688**, 137440 (2019).
- ²⁵ K. Tanaka, P. Arias, K. Hojo, T. Watanabe, M.E. Liao, A. Aleman, H. Zaid, M.S. Goorsky, and S.K. Kodambaka, Nano Lett. **23**, 4304–4310 (2023).
- ²⁶ J.E. Sader, J.W.M. Chon, and P. Mulvaney, Rev. Sci. Instrum. **70**, 3967–3969 (1999).
- ²⁷ M. Varenberg, I. Etsion, and G. Halperin, Rev. Sci. Instrum. **74**, 3362–3367 (2003).
- ²⁸ U.D. Schwarz, P. Köster, and R. Wiesendanger, Rev. Sci. Instrum. **67**, 2560–2567 (1996).
- ²⁹ K. Tanaka, et al., to be published.
- ³⁰ A. Deshpande, K. Hojo, K. Tanaka, P. Arias, H. Zaid, M. Liao, M. Goorsky, and S. Kodambaka, J. Vac. Sci. Technol. A **41**, 042203 (2023).
- ³¹ T. Demirbas, and M.Z. Baykara, J. Mater. Res. **31**, 1914–1923 (2016).
- ³² I. Szlufarska, M. Chandross, and R.W. Carpick, J. Phys. D: Appl. Phys. 41, 123001 (2008).
- ³³ J.M. Martin, C. Donnet, T. Le Mogne, T. Epicier, D.R. Wheeler, E.W. Roberts, and J. Moser, Phys. Rev. B **48**, 10583 (1993).
- ³⁴ M.R. Vazirisereshk, A. Martini, D.A. Strubbe, and M.Z. Baykara, Lubricants 7, (2019).
- ³⁵ P.D. Fleischauer, ASLE Trans. **27**, 82–88 (1984).